Supplementary material for V. T. Barone et al., Journal of Applied Physics 131, 205701 (2022)

Optoelectronic and mechanical properties of the orthogonal and tetragonal $Cu_2CdGe(S_xSe_{1-x})_4$ semiconducting system via first principles methods

V. T. Barone[a], B. B. Dumre[a], B. R. Tuttle[b], S. V. Khare[a,*]

[a]Department of Physics and Astronomy, and Wright Center for Photovoltaics Innovation and Commercialization (PVIC), University of Toledo, Toledo, OH 43606, USA

[b]Department of Physics, Penn State Behrend, Erie, PA 16563, USA

*Corresponding author: sanjay.khare@utoledo.edu

Supplementary material for V. T. Barone et al., Journal of Applied Physics 131, 205701 (2022)

x	e1	q1	e2	q2	e3	q3	e4	q4	e5	q5	e6	q6	e7	q7	e8	q8
0	Cd	0.71	Cd	0.71	Cu	0.36	Cu	0.36	Cu	0.36	Cu	0.36	Ge	0.85	Ge	0.85
0.125	Cd	0.71	Cd	0.75	Cu	0.36	Cu	0.39	Cu	0.36	Cu	0.39	Ge	0.93	Ge	0.85
0.25	Cd	0.75	Cd	0.75	Cu	0.36	Cu	0.43	Cu	0.36	Cu	0.43	Ge	0.93	Ge	0.93
0.375	Cd	0.79	Cd	0.75	Cu	0.36	Cu	0.46	Cu	0.36	Cu	0.46	Ge	0.94	Ge	1.02
0.5	Cd	0.79	Cd	0.79	Cu	0.36	Cu	0.48	Cu	0.36	Cu	0.48	Ge	1.02	Ge	1.02
0.625	Cd	0.82	Cd	0.79	Cu	0.39	Cu	0.48	Cu	0.39	Cu	0.48	Ge	1.02	Ge	1.10
0.75	Cd	0.82	Cd	0.82	Cu	0.43	Cu	0.48	Cu	0.43	Cu	0.48	Ge	1.11	Ge	1.11
0.875	Cd	0.82	Cd	0.86	Cu	0.46	Cu	0.48	Cu	0.46	Cu	0.48	Ge	1.20	Ge	1.11
1	Cd	0.86	Cd	0.86	Cu	0.48	Cu	0.48	Cu	0.48	Cu	0.48	Ge	1.20	Ge	1.20

x	e9	q9	e10	q10	e11	q11	e12	q12	e13	q13	e14	q14	e15	q15	e16	q16
0	Se	-0.57	Se	-0.57	Se	-0.57	Se	-0.57	Se	-0.57	Se	-0.57	Se	-0.57	Se	-0.57
0.125	Se	-0.57	Se	-0.57	Se	-0.57	Se	-0.57	Se	-0.57	Se	-0.57	Se	-0.57	S	-0.75
0.25	Se	-0.57	Se	-0.57	Se	-0.57	Se	-0.57	Se	-0.57	Se	-0.57	S	-0.75	S	-0.76
0.375	Se	-0.57	Se	-0.57	Se	-0.57	Se	-0.57	Se	-0.58	S	-0.76	S	-0.76	S	-0.76
0.5	Se	-0.57	Se	-0.57	Se	-0.57	Se	-0.57	S	-0.76	S	-0.76	S	-0.76	S	-0.76
0.625	Se	-0.57	Se	-0.57	Se	-0.57	S	-0.75	S	-0.76	S	-0.76	S	-0.76	S	-0.76
0.75	Se	-0.57	Se	-0.57	S	-0.76	S	-0.76	S	-0.76	S	-0.76	S	-0.76	S	-0.76
0.875	Se	-0.57	S	-0.76	S	-0.76	S	-0.76	S	-0.76	S	-0.76	S	-0.76	S	-0.75
1	S	-0.76	S	-0.76	S	-0.76	S	-0.76	S	-0.76	S	-0.76	S	-0.76	S	-0.76

Table SI. Effective charges computed through Bader charge analysis for t-$Cu_2CdGe(S_xSe_{1-x})_4$. 'eN' represents the element located at site *N*, and 'qN' is the effective charge of the element at site *N* (in units of the electron charge *e*).

x	e1	q1	e2	q2	e3	q3	e4	q4	e5	q5	e6	q6	e7	q7	e8	q8
0	Cd	0.71	Cd	0.71	Cu	0.36	Cu	0.36	Cu	0.36	Cu	0.36	Ge	0.85	Ge	0.85
0.125	Cd	0.71	Cd	0.75	Cu	0.36	Cu	0.40	Cu	0.40	Cu	0.36	Ge	0.93	Ge	0.86
0.25	Cd	0.75	Cd	0.75	Cu	0.36	Cu	0.44	Cu	0.40	Cu	0.40	Ge	1.01	Ge	0.86
0.375	Cd	0.75	Cd	0.79	Cu	0.35	Cu	0.47	Cu	0.40	Cu	0.43	Ge	1.02	Ge	0.94
0.5	Cd	0.75	Cd	0.82	Cu	0.39	Cu	0.46	Cu	0.39	Cu	0.47	Ge	1.10	Ge	0.95
0.625	Cd	0.78	Cd	0.82	Cu	0.43	Cu	0.46	Cu	0.39	Cu	0.50	Ge	1.11	Ge	1.03
0.75	Cd	0.78	Cd	0.86	Cu	0.46	Cu	0.46	Cu	0.42	Cu	0.49	Ge	1.11	Ge	1.12
0.875	Cd	0.82	Cd	0.86	Cu	0.49	Cu	0.46	Cu	0.46	Cu	0.49	Ge	1.20	Ge	1.12
1	Cd	0.86	Cd	0.86	Cu	0.49	Cu	0.49	Cu	0.49	Cu	0.49	Ge	1.21	Ge	1.21

x	e9	q9	e10	q10	e11	q11	e12	q12	e13	q13	e14	q14	e15	q15	e16	q16
0	Se	-0.58	Se	-0.57	Se	-0.57	Se	-0.58	Se	-0.58	Se	-0.57	Se	-0.57	Se	-0.58
0.125	Se	-0.58	Se	-0.57	Se	-0.57	Se	-0.58	Se	-0.58	Se	-0.57	Se	-0.57	S	-0.76
0.25	Se	-0.58	Se	-0.56	Se	-0.57	Se	-0.59	Se	-0.58	Se	-0.57	S	-0.75	S	-0.76
0.375	Se	-0.59	Se	-0.56	Se	-0.57	Se	-0.59	Se	-0.59	S	-0.75	S	-0.75	S	-0.76
0.5	Se	-0.59	Se	-0.56	Se	-0.57	Se	-0.59	S	-0.76	S	-0.76	S	-0.75	S	-0.76
0.625	Se	-0.59	Se	-0.56	Se	-0.57	S	-0.77	S	-0.76	S	-0.75	S	-0.75	S	-0.77
0.75	Se	-0.59	Se	-0.56	S	-0.75	S	-0.77	S	-0.76	S	-0.75	S	-0.75	S	-0.77
0.875	Se	-0.59	S	-0.75	S	-0.75	S	-0.77	S	-0.77	S	-0.75	S	-0.75	S	-0.77
1	S	-0.77	S	-0.75	S	-0.75	S	-0.77	S	-0.77	S	-0.75	S	-0.75	S	-0.77

Table SII. Effective charges computed through Bader charge analysis for o-$Cu_2CdGe(S_xSe_{1-x})_4$**.** 'eN' represents the element located at site *N*, and 'qN' is the effective charge of the element at site *N* (in units of the electron charge *e*).

		t-$Cu_2CdGe(S_xSe_{1-x})_4$				o-$Cu_2CdGe(S_xSe_{1-x})_4$			
x	A	Se-A Pairs	⟨Se-A⟩ Dist.	S-A Pairs	⟨S-A⟩ Dist.	Se-A Pairs	⟨Se-A⟩ Dist.	S-A Pairs	⟨S-A⟩ Dist.
0.000	Cu	16	2.44	0	–	16	2.44	0	–
	Cd	8	2.70	0	–	8	2.70	0	–
	Ge	8	2.46	0	–	8	2.45	0	–
0.125	Cu	14	2.44	2	2.30	14	2.45	2	2.29
	Cd	7	2.69	1	2.61	7	2.70	1	2.59
	Ge	7	2.45	1	2.33	7	2.44	1	2.33
0.250	Cu	12	2.44	4	2.31	12	2.45	4	2.30
	Cd	6	2.69	2	2.60	6	2.69	2	2.60
	Ge	6	2.45	2	2.32	6	2.44	2	2.32
0.375	Cu	10	2.44	6	2.33	10	2.45	6	2.31
	Cd	5	2.68	3	2.60	5	2.69	3	2.61
	Ge	5	2.44	3	2.32	5	2.44	3	2.31
0.500	Cu	8	2.42	8	2.34	8	2.46	8	2.31
	Cd	4	2.67	4	2.60	4	2.68	4	2.59
	Ge	4	2.44	4	2.31	4	2.43	4	2.31
0.625	Cu	6	2.44	10	2.32	6	2.46	10	2.32
	Cd	3	2.67	5	2.59	3	2.68	5	2.59
	Ge	3	2.43	5	2.31	3	2.42	5	2.30
0.750	Cu	4	2.45	12	2.32	4	2.47	12	2.31
	Cd	2	2.66	6	2.58	2	2.67	6	2.59
	Ge	2	2.42	6	2.30	2	2.41	6	2.30
0.875	Cu	2	2.46	14	2.32	2	2.47	14	2.32
	Cd	1	2.65	7	2.58	1	2.67	7	2.58
	Ge	1	2.42	7	2.30	1	2.41	7	2.29
1.000	Cu	0	–	16	2.32	0	–	16	2.32
	Cd	0	–	8	2.57	0	–	8	2.58
	Ge	0	–	8	2.29	0	–	8	2.29

Table SIII. Nearest neighbor counts and average distances (in Å) between anions (Se, S) and cations (A = Cu, Cd, Ge) in tetragonal (t-) and orthorhombic (o-) $Cu_2CdGe(S_xSe_{1-x})_4$.

x	C_{11}	C_{22}	C_{33}	C_{44}	C_{55}	C_{66}	C_{12}	C_{13}	C_{23}
0.000	76	76	77	31	31	33	48	46	46
0.125	78	78	73	32	32	33	49	48	48
0.250	79	80	73	32	33	34	50	48	48
0.375	81	82	75	33	33	35	52	50	50
0.500	83	83	77	34	34	36	52	51	51
0.625	90	90	79	35	35	38	54	51	51
0.750	89	88	82	36	37	39	56	54	53
0.875	92	92	85	37	37	40	58	55	55
1.000	93	93	88	38	38	41	60	56	56

Table SIV Elastic constants for tetragonal $Cu_2CdGe(S_xSe_{1-x})_4$ (in GPa).

x	C_{11}	C_{22}	C_{33}	C_{44}	C_{55}	C_{66}	C_{12}	C_{13}	C_{23}
0.000	104	84	89	22	20	18	32	36	43
0.125	108	86	92	22	20	19	33	35	44
0.250	109	86	89	22	21	19	34	35	45
0.375	112	89	90	22	21	20	36	37	45
0.500	115	92	99	24	21	20	36	38	47
0.625	119	94	100	23	22	21	38	38	47
0.750	122	96	99	25	23	22	38	39	48
0.875	124	98	102	25	23	22	39	42	51
1.000	129	103	109	26	24	22	42	43	52

Table SV. Elastic constants for orthorhombic $Cu_2CdGe(S_xSe_{1-x})_4$ (in GPa).

	t- $Cu_2CdGe(S_xSe_{1-x})_4$		o- $Cu_2CdGe(S_xSe_{1-x})_4$	
x	E_g	E_F	E_g	E_F
0.000	1.2, (1.1)[j], (1.3)[g], (1.2)[f]	2.2	1.3, (1.3)[b,j], (1.2)[c]	2.2
0.125	1.2	2.3	1.3, (1.4)[b*]	2.3
0.250	1.3	2.4	1.4, (1.5)[b*]	2.4
0.375	1.4	2.5	1.5, (1.6)[b*]	2.5
0.500	1.4	2.6	1.6, (1.7)[b*]	2.6
0.625	1.5	2.8	1.6, (1.8)[b*]	2.7
0.750	1.6	2.9	1.7, (1.9)[b*]	2.9
0.875	1.7	3.0	1.7, (1.9)[b*]	3.0
1.000	1.8, (1.8)[f]	3.1	1.9, (2.0)[b,d]	3.1

Table SVI. Bandgaps (E_g) and Fermi energies (E_F) for tetragonal (t-) and orthorhombic (o-) $Cu_2CdGe(S_xSe_{1-x})_4$, both in units of eV.

Experimental References: (b): [1], (c): [2], (d): [3], (j): [4]

b*: Linear interpolations (Ref [1]'s step size was $\Delta x = 0.2$, while ours was $\Delta x = 0.125$)

Theoretical References: (g): [5], (f): [6]

	t-$Cu_2CdGe(S_xSe_{1-x})_4$			o-$Cu_2CdGe(S_xSe_{1-x})_4$		
x	$-m_h^*/m_0$	m_e^*/m_0	$\hat{\mathbf{u}}$	$-m_h^*/m_0$	m_e^*/m_0	$\hat{\mathbf{u}}$
0.000	0.8	0.2	$(1,0,0)$	1.4	0.2	$(1,0,0)$
	0.8	0.2	$(0,1,0)$	1.4	0.2	$(0,1,0)$
	0.5	0.1	$(0,0,1)$	0.8	0.2	$(0,0,1)$
0.125	0.8	0.2	$(1,0,0)$	1.4	0.2	$(1,0,0)$
	0.8	0.2	$(0,1,0)$	1.4	0.2	$(0,1,0)$
	0.5	0.1	$(0,0,1)$	0.8	0.2	$(0,0,1)$
0.250	0.7	0.2	$(1,0,0)$	1.4	0.2	$(1,0,0)$
	0.8	0.2	$(0,1,0)$	1.5	0.2	$(0,1,0)$
	0.6	0.1	$(0,0,1)$	0.7	0.2	$(0,0,1)$
0.375	0.8	0.2	$(1,0,0)$	1.6	0.2	$(1,0,0)$
	0.8	0.2	$(0,1,0)$	1.7	0.2	$(0,1,0)$
	0.7	0.1	$(0,0,1)$	0.8	0.2	$(0,0,1)$
0.500	0.8	0.2	$(1,0,0)$	1.7	0.2	$(1,0,0)$
	0.8	0.2	$(0,1,0)$	1.4	0.2	$(0,1,0)$
	0.7	0.1	$(0,0,1)$	0.9	0.2	$(0,0,1)$
0.625	0.8	0.2	$(1,0,0)$	1.5	0.2	$(1,0,0)$
	0.8	0.2	$(0,1,0)$	1.7	0.2	$(0,1,0)$
	0.7	0.2	$(0,0,1)$	0.9	0.2	$(0,0,1)$
0.750	0.8	0.2	$(1,0,0)$	1.5	0.2	$(1,0,0)$
	0.8	0.2	$(0,1,0)$	1.9	0.2	$(0,1,0)$
	0.7	0.2	$(0,0,1)$	0.7	0.2	$(0,0,1)$
0.875	0.8	0.2	$(1,0,0)$	1.5	0.2	$(1,0,0)$
	0.8	0.2	$(0,1,0)$	2.0	0.2	$(0,1,0)$
	0.8	0.2	$(0,0,1)$	0.8	0.2	$(0,0,1)$
1.000	0.8	0.2	$(1,0,0)$	1.6	0.2	$(1,0,0)$
	0.8	0.2	$(0,1,0)$	1.7	0.2	$(0,1,0)$
	0.6	0.2	$(0,0,1)$	0.8	0.2	$(0,0,1)$

Table SVII. Effective carrier masses of holes (m_h^*) and electrons (m_e^*) in tetragonal (t-) and orthorhombic (o-) $Cu_2CdGe(S_xSe_{1-x})_4$, normalized to m_0 – the electron rest mass. The fractional reciprocal-space unit vectors originating from the band extrema (at Γ in all cases) are listed as $\hat{\mathbf{u}} = (u_a, u_b, u_c)$.

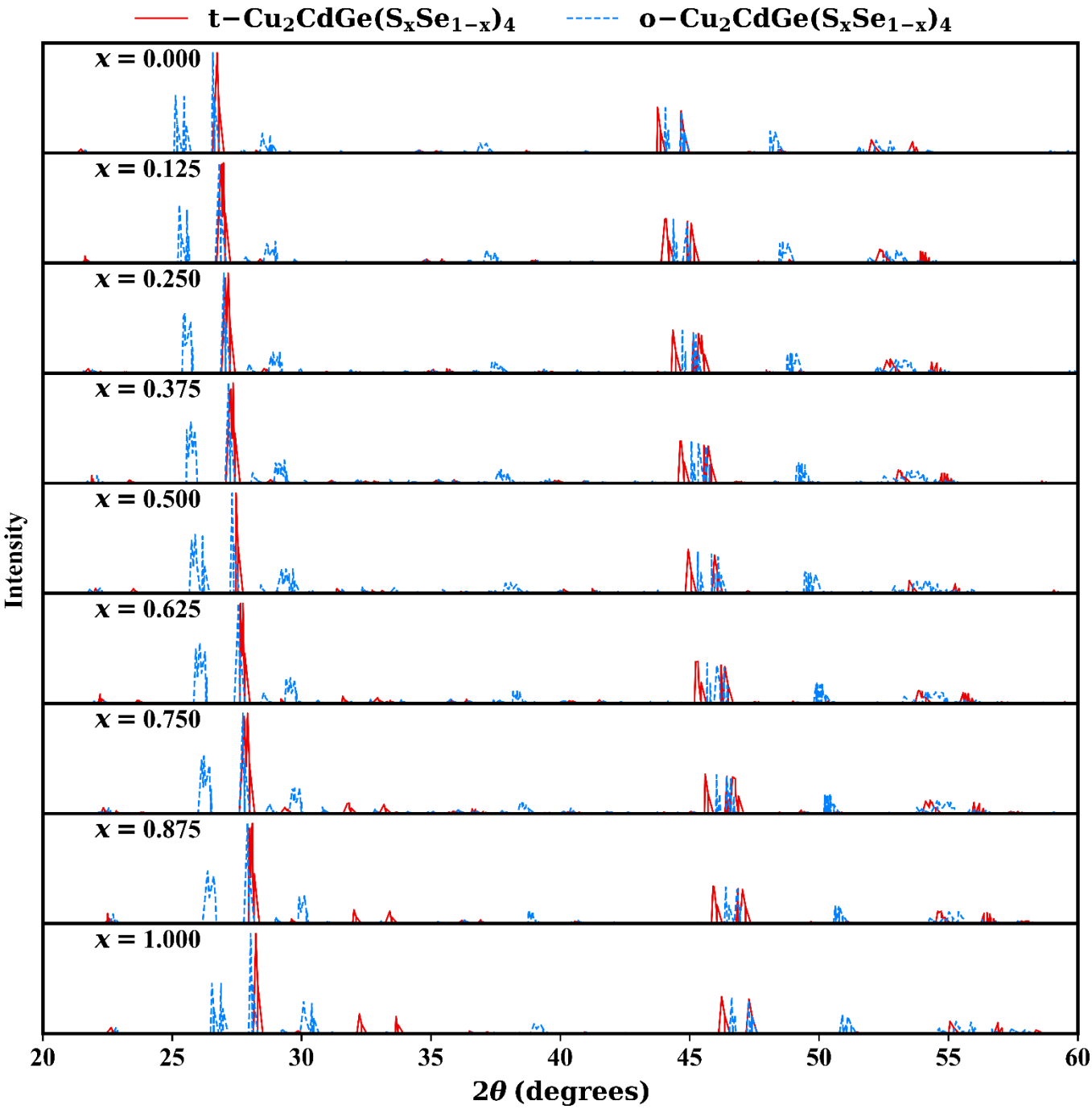

Figure S1. Powder diffraction patterns for tetragonal (t-) and orthorhombic (o-) $Cu_2CdGe(S_xSe_{1-x})_4$ simulated using the VESTA program. Plotting points are generated using two waves of λ = 1.541 Å, 1.544 Å with relative intensities 1.0 and 0.5. Spikes are widened by 0.2° at their bases for visibility. Rightward shifts in peak locations with increasing x, are attributed to shrinking cell parameters.

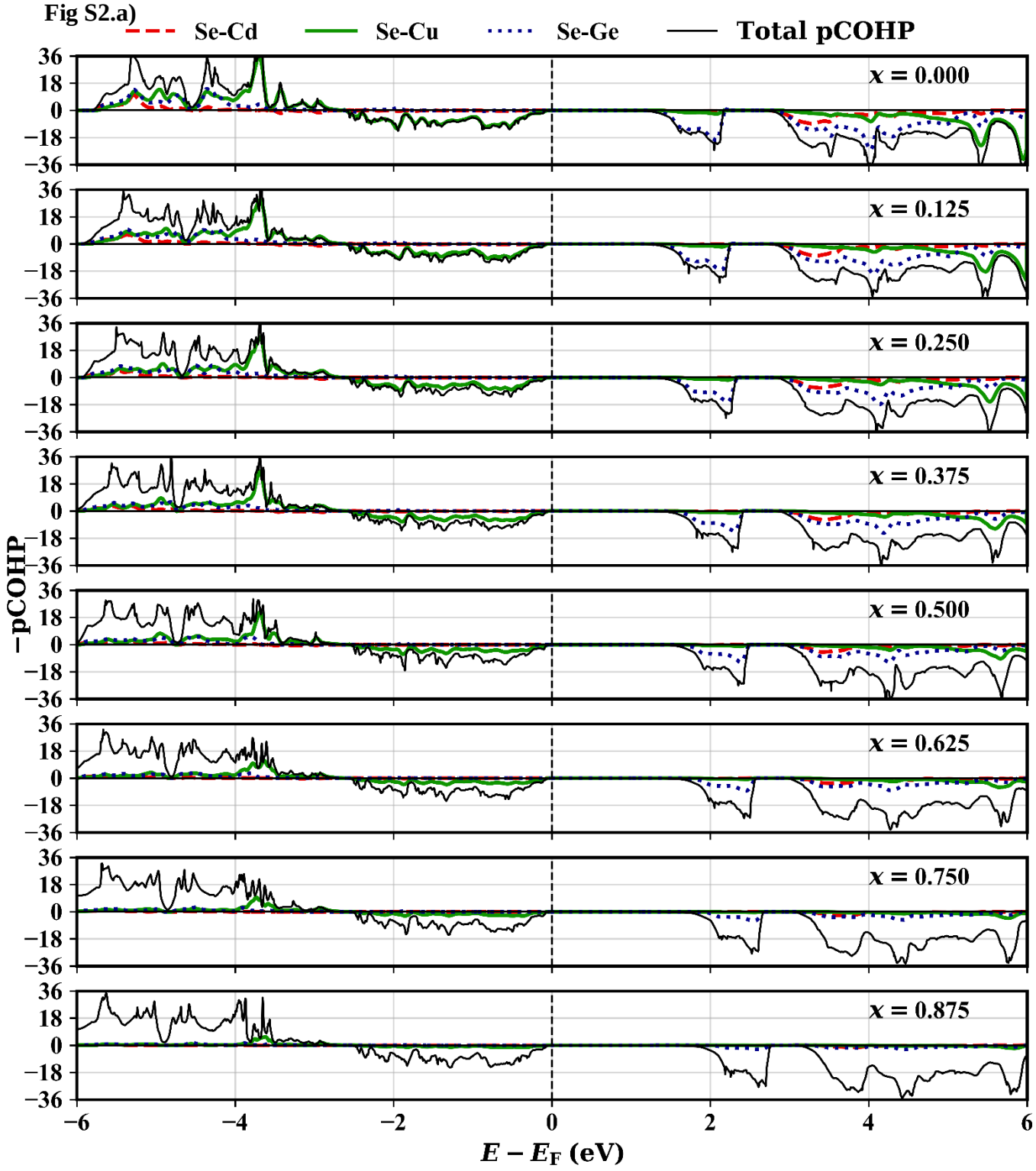

Figure S2 (a-d). COHP plots for tetra (t-) and orthorhombic (o-) $Cu_2CdGe(S_xSe_{1-x})_4$. The black line shows the total COHP of all pairs. **(a)** Se-(Cu/Cd/Ge) pairs for the t-phase, **(b)** S-(Cu/Cd/Ge) pairs for the t-phase, **(c)** Se-(Cu/Cd/Ge) pairs for the o-phase, **(d)** S-(Cu/Cd/Ge) pairs for o-phase.

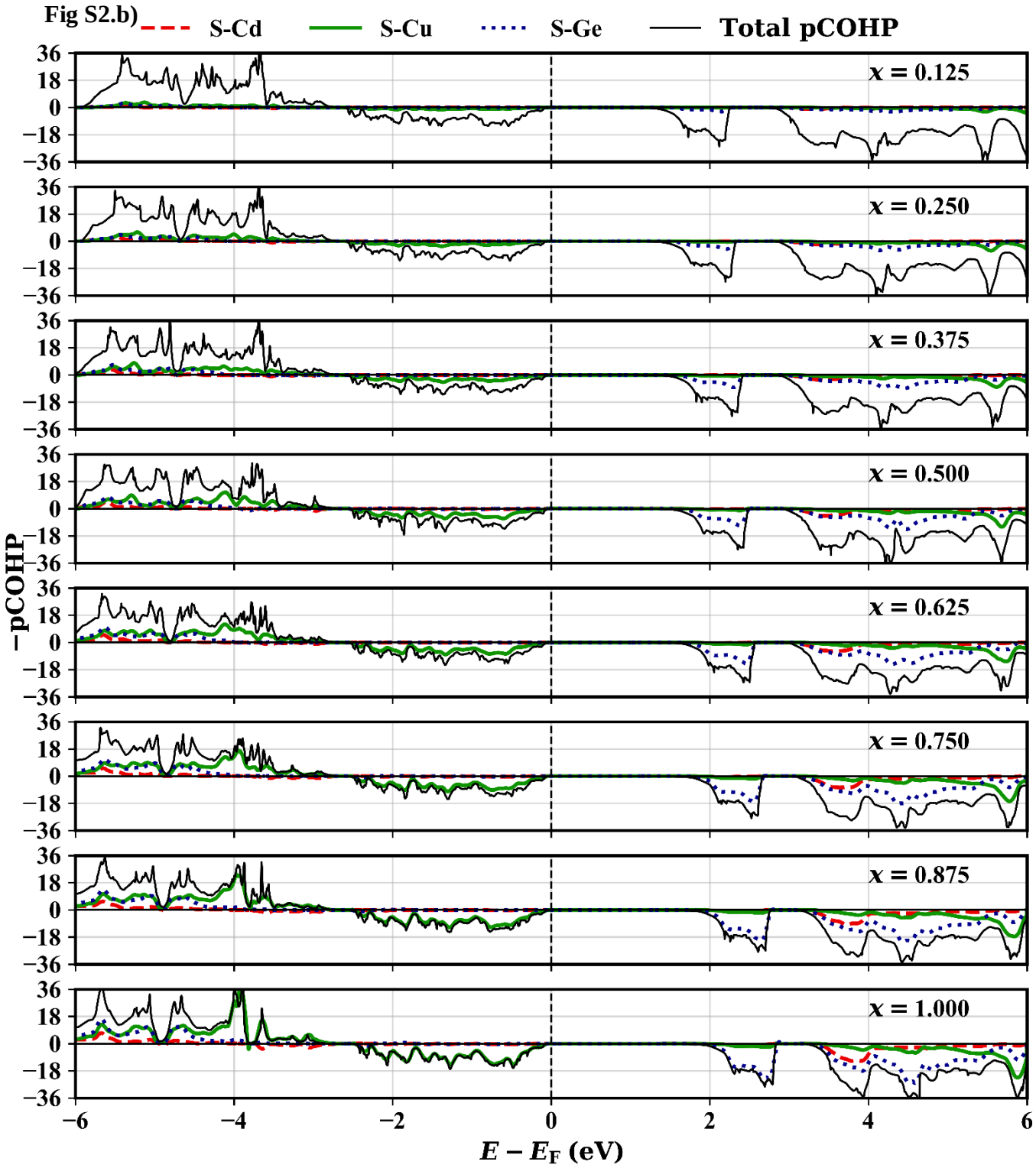
Fig S2.b)
S-Cd
S-Cu
S-Ge
Total pCOHP
x = 0.125
x = 0.250
x = 0.375
x = 0.500
x = 0.625
x = 0.750
x = 0.875
x = 1.000
−pCOHP
E − E_F (eV)

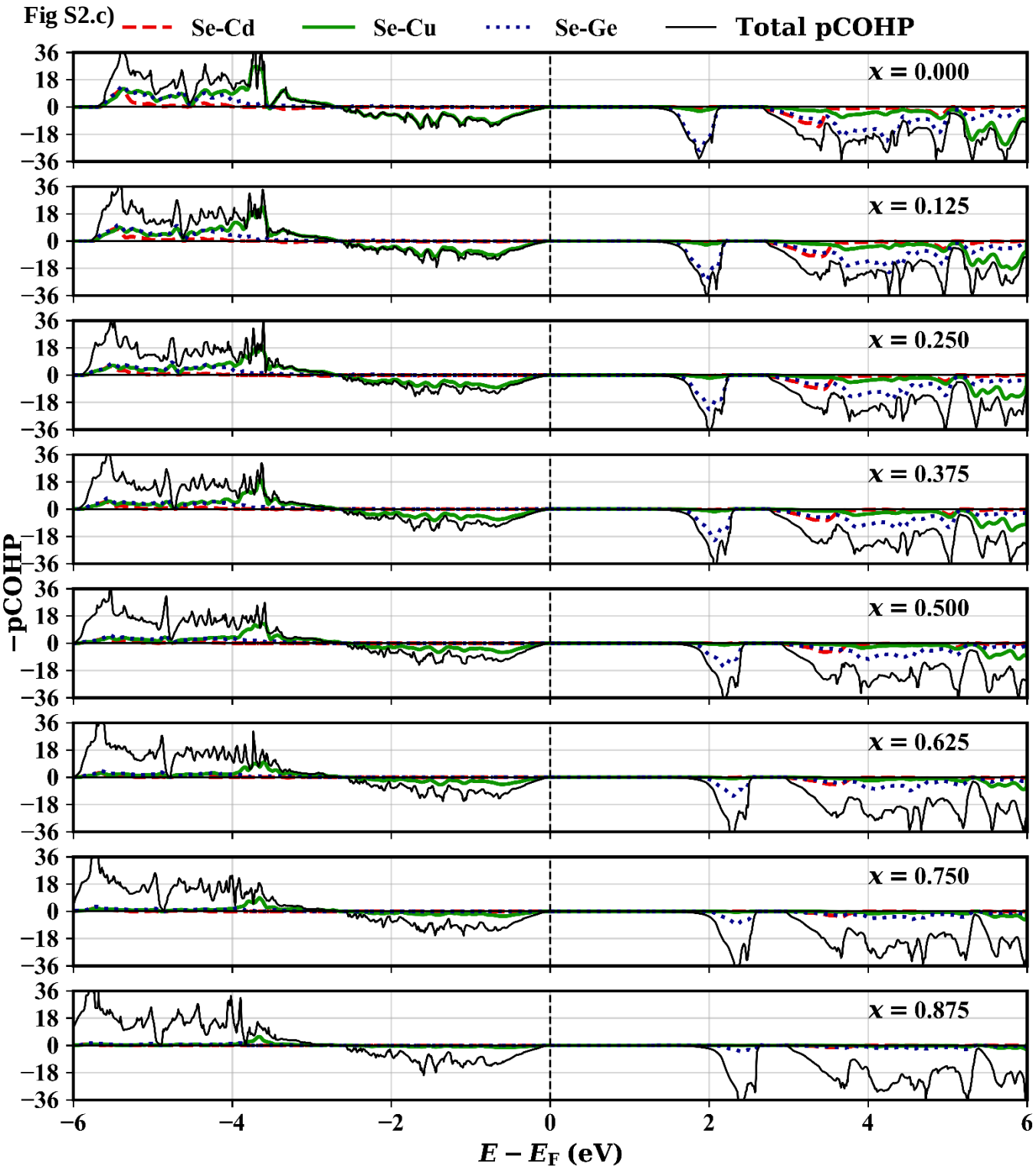
Fig S2.c)
Se-Cd
Se-Cu
Se-Ge
Total pCOHP
x = 0.000
x = 0.125
x = 0.250
x = 0.375
x = 0.500
x = 0.625
x = 0.750
x = 0.875
−pCOHP
36
18
0
−18
−36
−6
−4
−2
0
2
4
6
E − E_F (eV)

Fig S2.d)

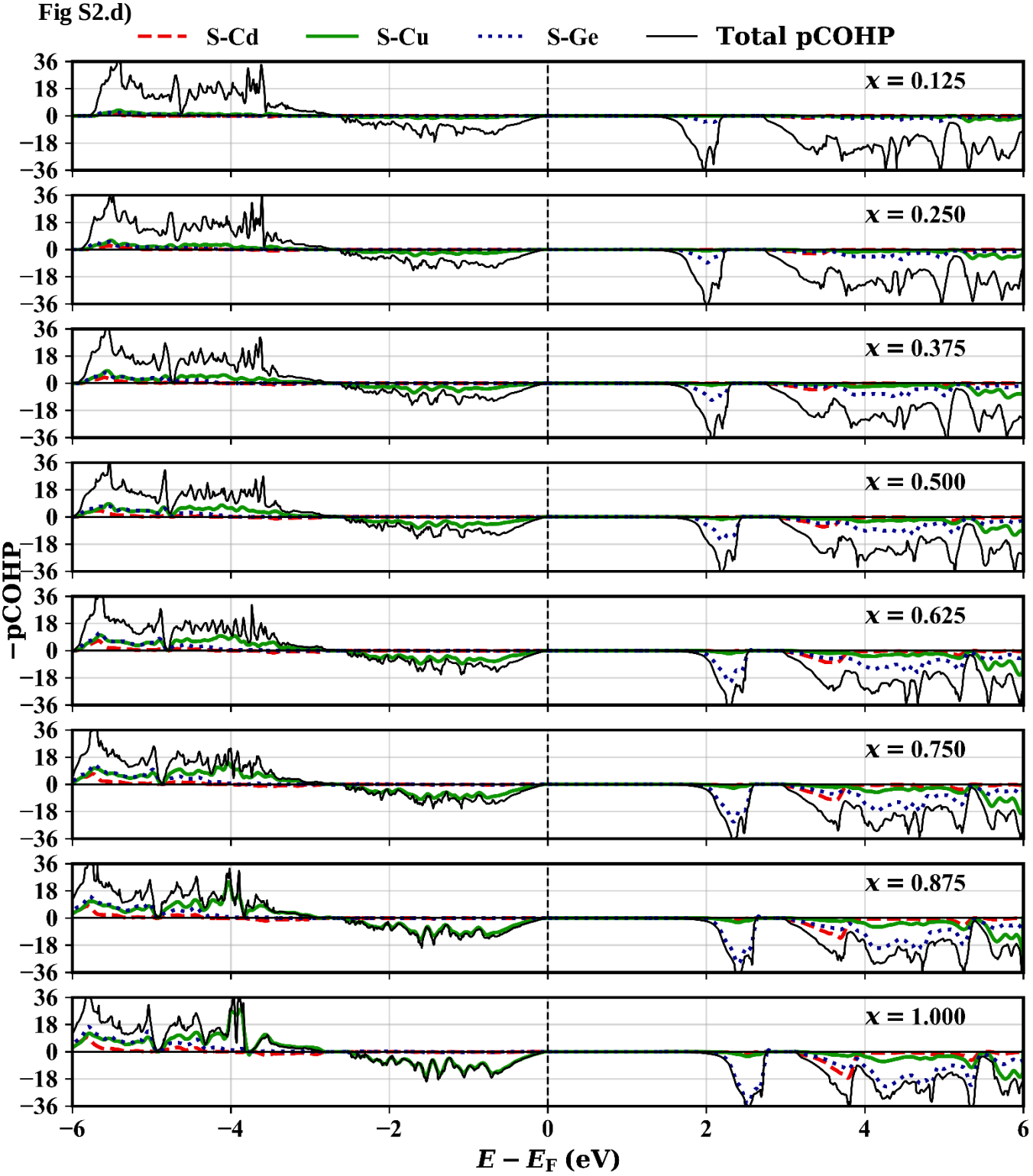
S-Cd
S-Cu
S-Ge
Total pCOHP
x = 0.125
x = 0.250
x = 0.375
x = 0.500
x = 0.625
x = 0.750
x = 0.875
x = 1.000
−pCOHP
36
18
0
−18
−36
−6
−4
−2
0
2
4
6
E − E_F (eV)

Figure S3.a)

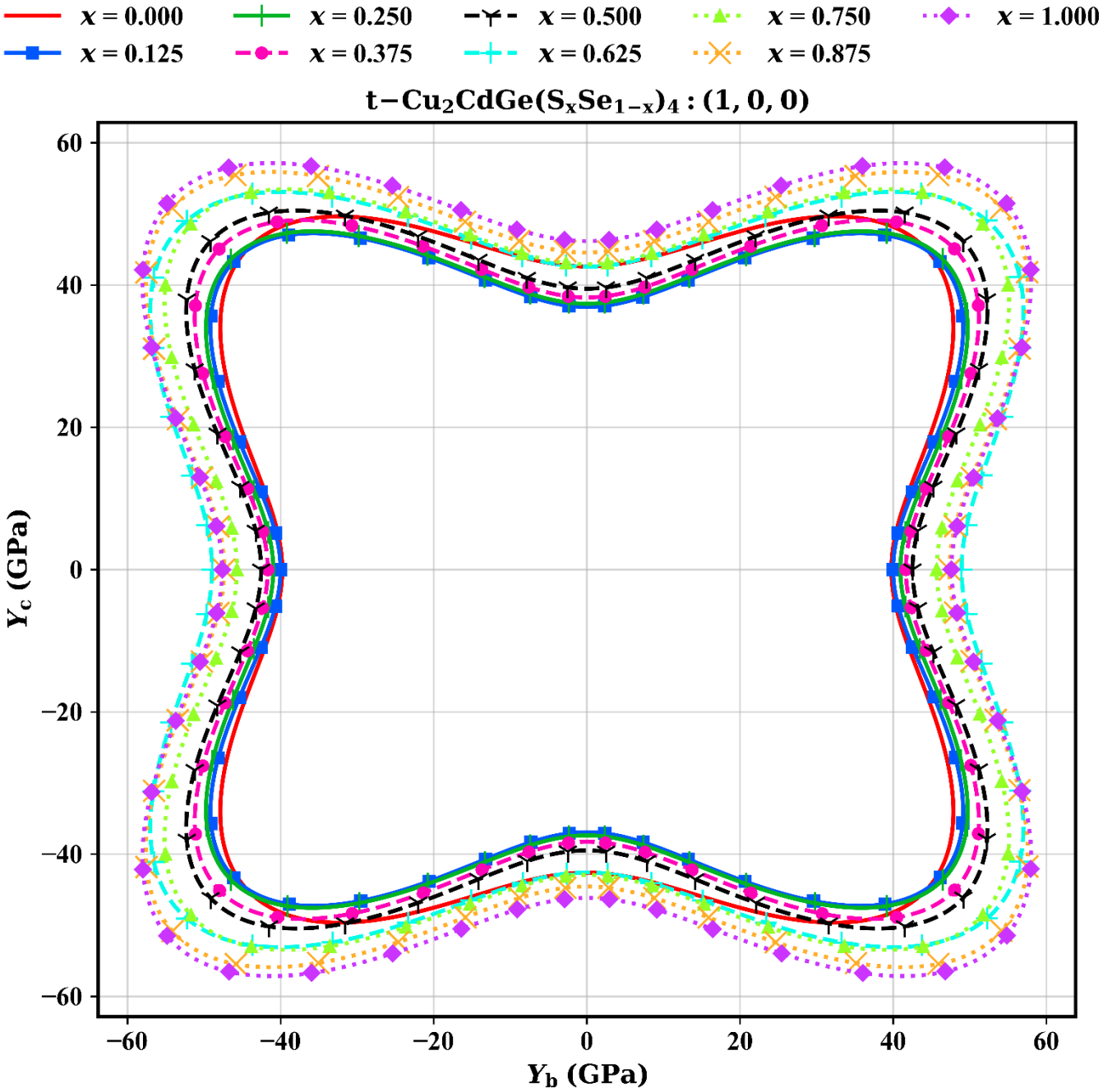

Figure S3 (a-f). 2D representations of the directional dependence of the Young's Modulus Y in $Cu_2CdGe(S_xSe_{1-x})_4$. Slices are on planes located at the origin normal to either the a, b, or c direction. **(a-c)** are for tetragonal (t-) $Cu_2CdGe(S_xSe_{1-x})_4$ and **(d-f)** are for orthorhombic (o-) $Cu_2CdGe(S_xSe_{1-x})_4$.

Figure S3.b)

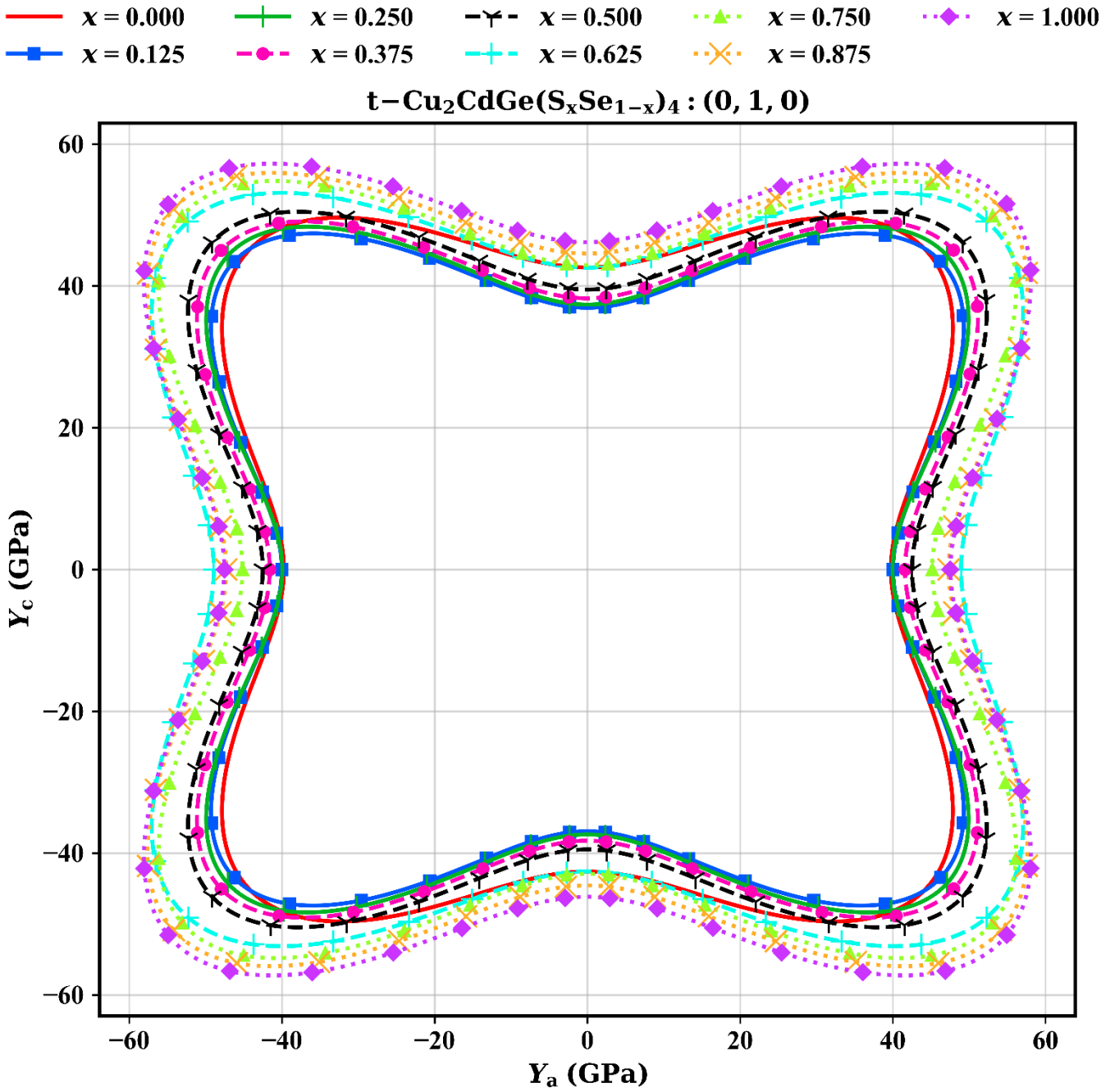
x = 0.000
x = 0.125
x = 0.250
x = 0.375
x = 0.500
x = 0.625
x = 0.750
x = 0.875
x = 1.000
t−Cu2CdGe(SxSe1−x)4 : (0, 1, 0)
Yc (GPa)
Ya (GPa)
60
40
20
0
−20
−40
−60

Figure S3.c)

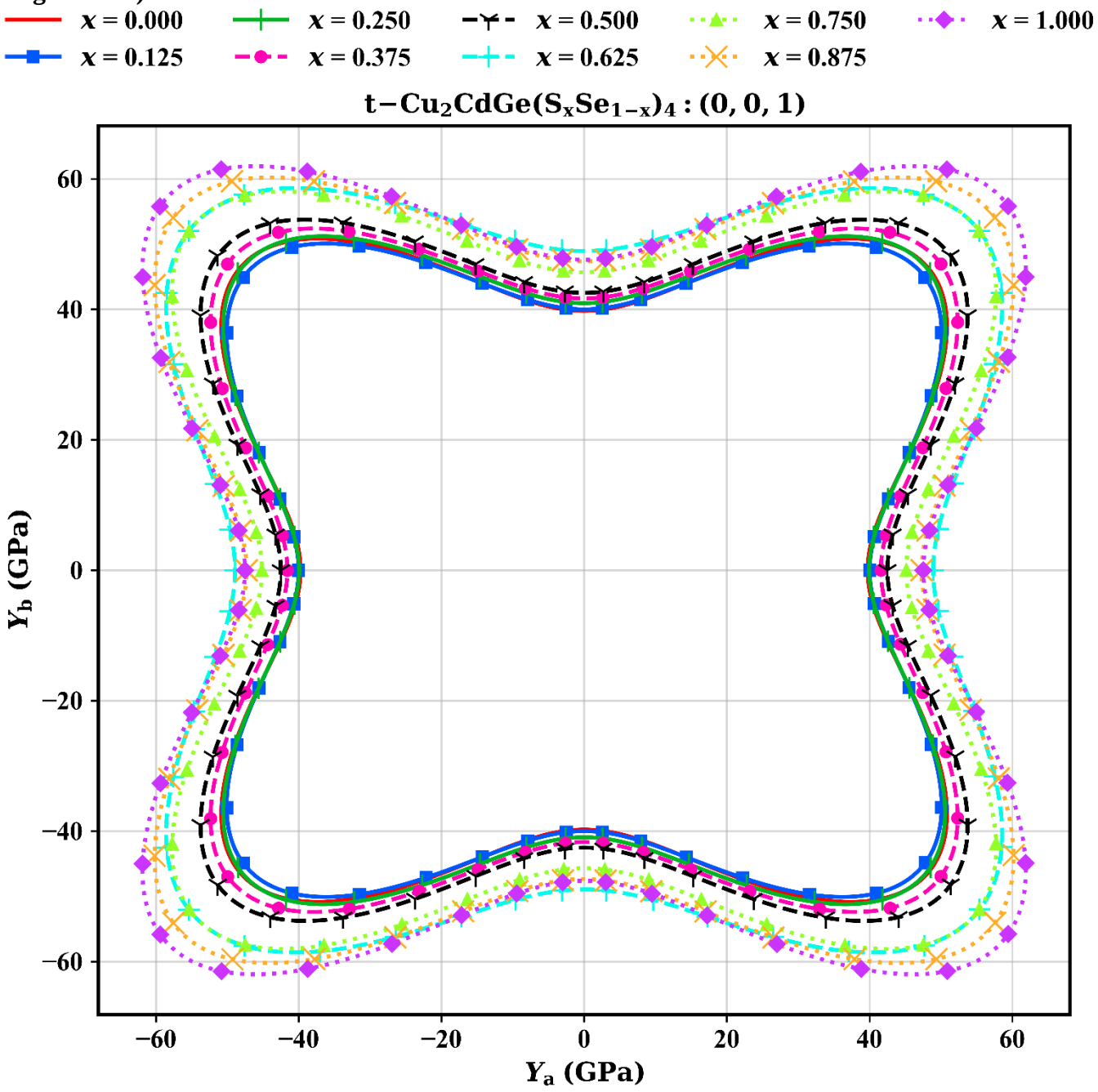
x = 0.000
x = 0.125
x = 0.250
x = 0.375
x = 0.500
x = 0.625
x = 0.750
x = 0.875
x = 1.000
t−Cu2CdGe(SxSe1−x)4 : (0, 0, 1)
Yb (GPa)
Ya (GPa)
60
40
20
0
−20
−40
−60
−60
−40
−20
0
20
40
60

Figure S3.d)

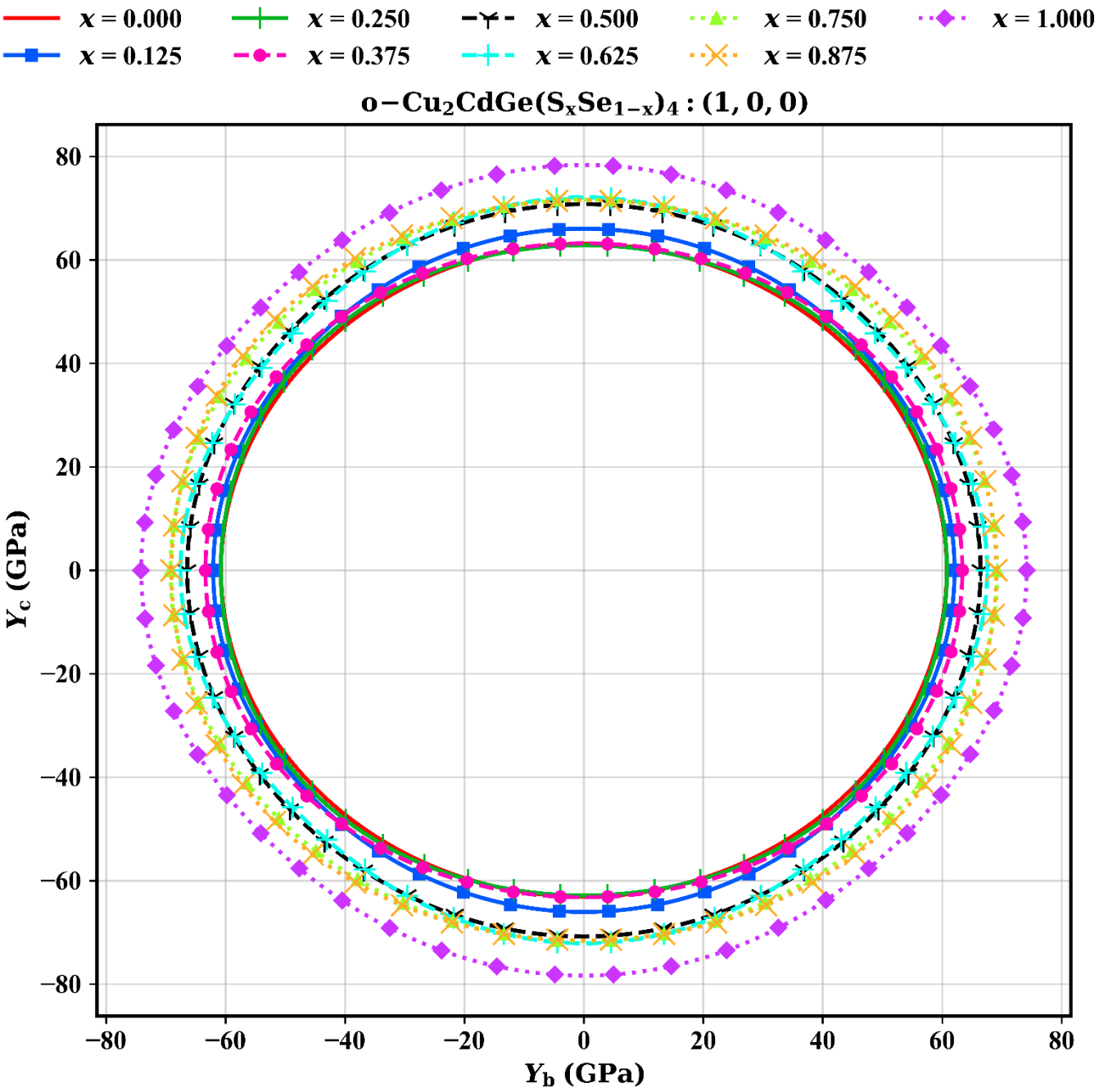
x = 0.000
x = 0.125
x = 0.250
x = 0.375
x = 0.500
x = 0.625
x = 0.750
x = 0.875
x = 1.000
o−Cu2CdGe(SxSe1−x)4 : (1, 0, 0)
Yc (GPa)
Yb (GPa)
80
60
40
20
0
−20
−40
−60
−80

Figure S3.e)

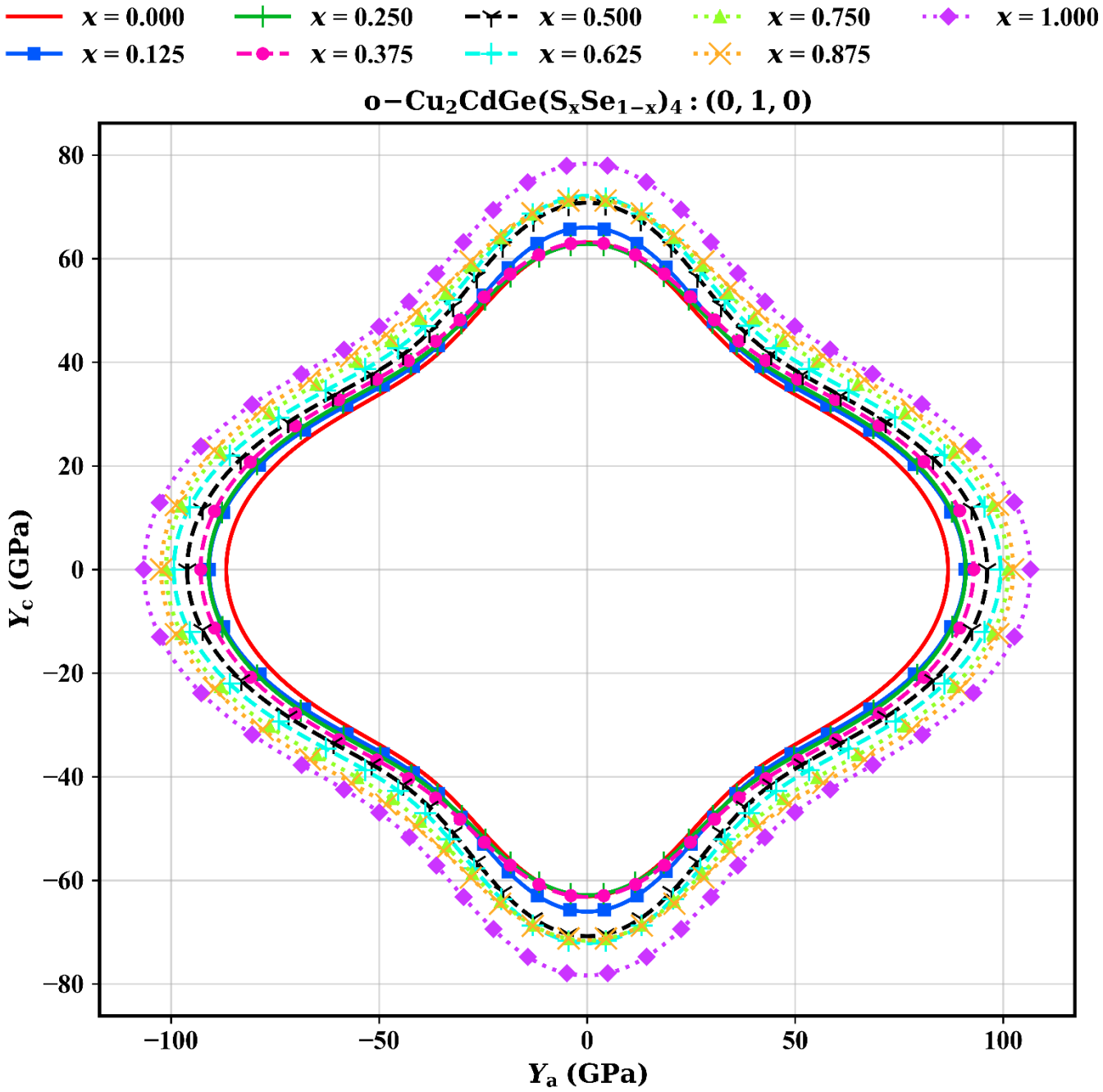
x = 0.000
x = 0.125
x = 0.250
x = 0.375
x = 0.500
x = 0.625
x = 0.750
x = 0.875
x = 1.000
o−Cu2CdGe(SxSe1−x)4 : (0, 1, 0)
Yc (GPa)
Ya (GPa)
80
60
40
20
0
−20
−40
−60
−80
−100
−50
0
50
100

Figure S3.f)

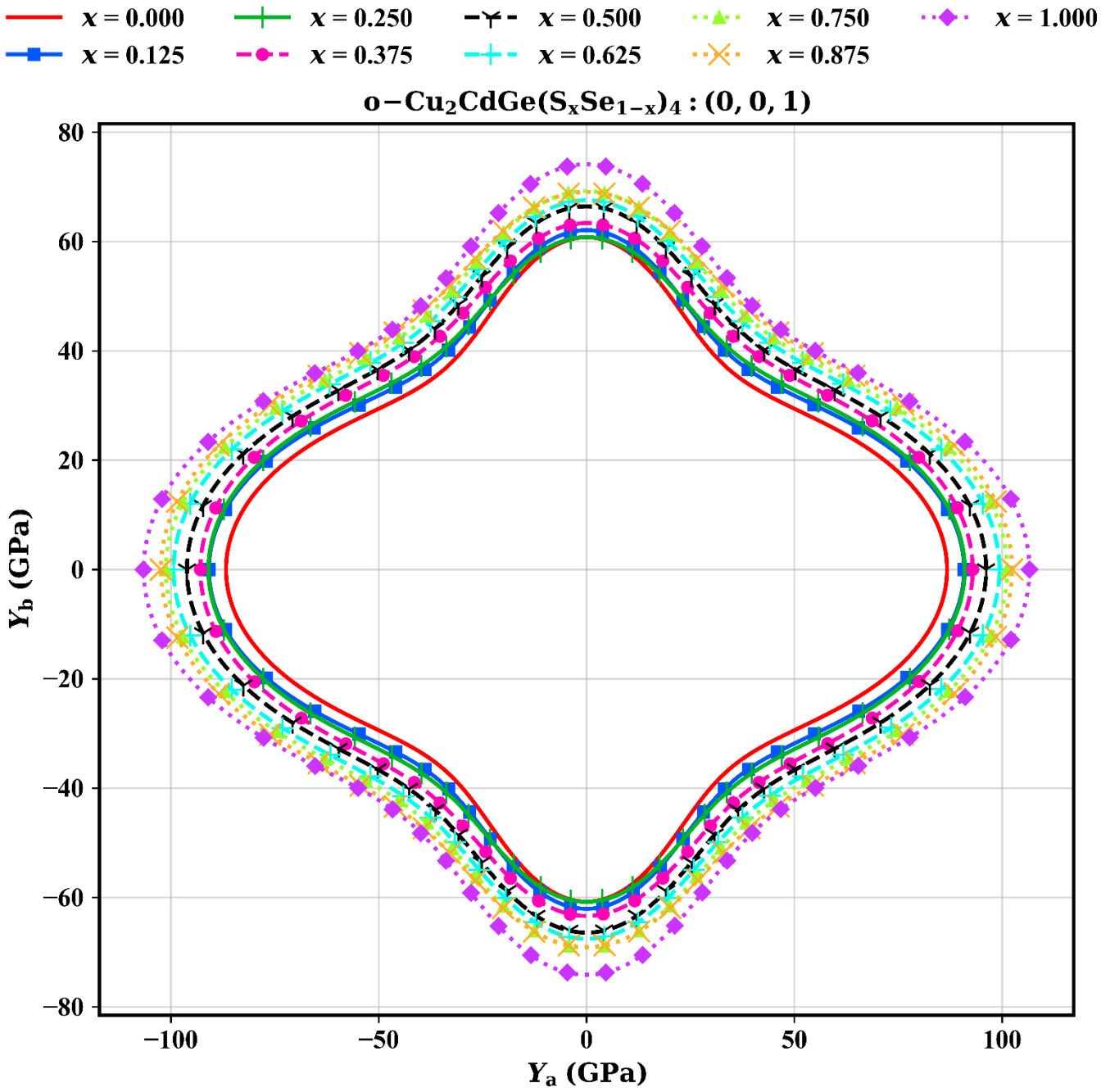
x = 0.000
x = 0.125
x = 0.250
x = 0.375
x = 0.500
x = 0.625
x = 0.750
x = 0.875
x = 1.000
o−Cu2CdGe(SxSe1−x)4 : (0, 0, 1)
Yb (GPa)
Ya (GPa)
80
60
40
20
0
−20
−40
−60
−80
−100
−50
0
50
100

Figure S4.a)

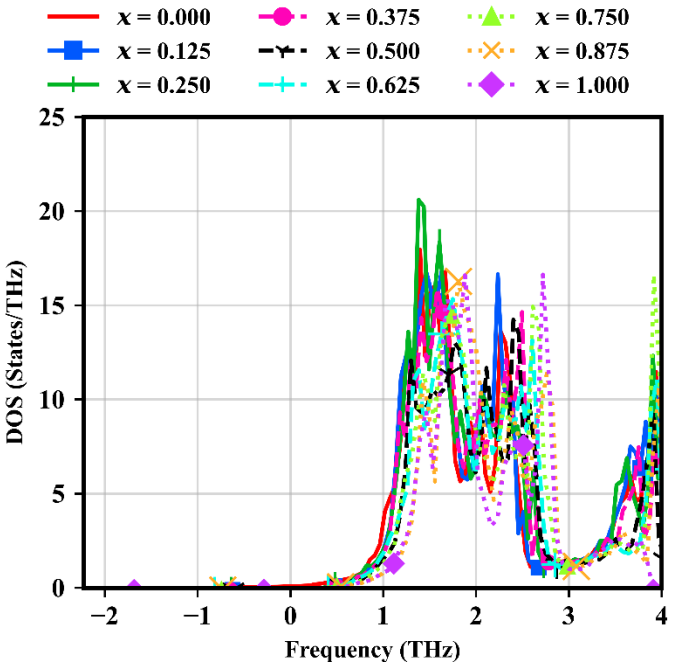

Figure S4.b)

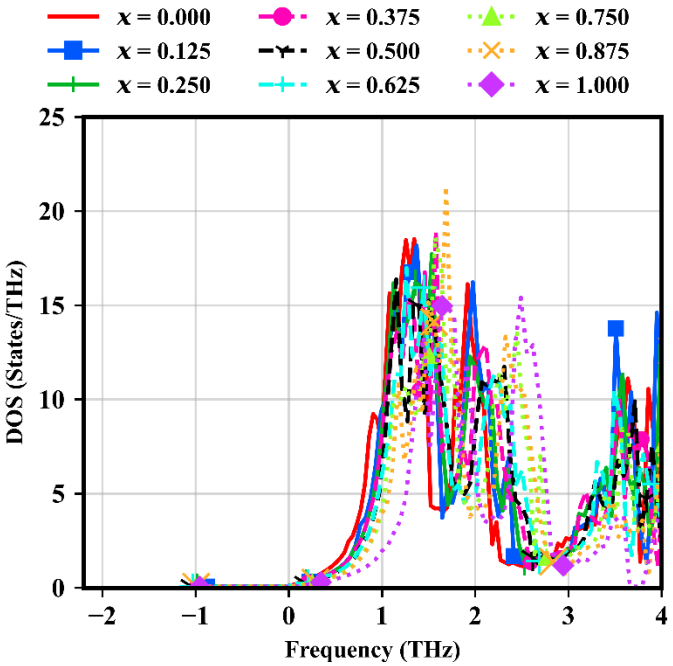

Figure S4(a-b). Phonon DOS of the **(a)** tetragonal and **(b)** orthorhombic phases plotted for low absolute values of frequency. The negative frequencies represent the imaginary axis.

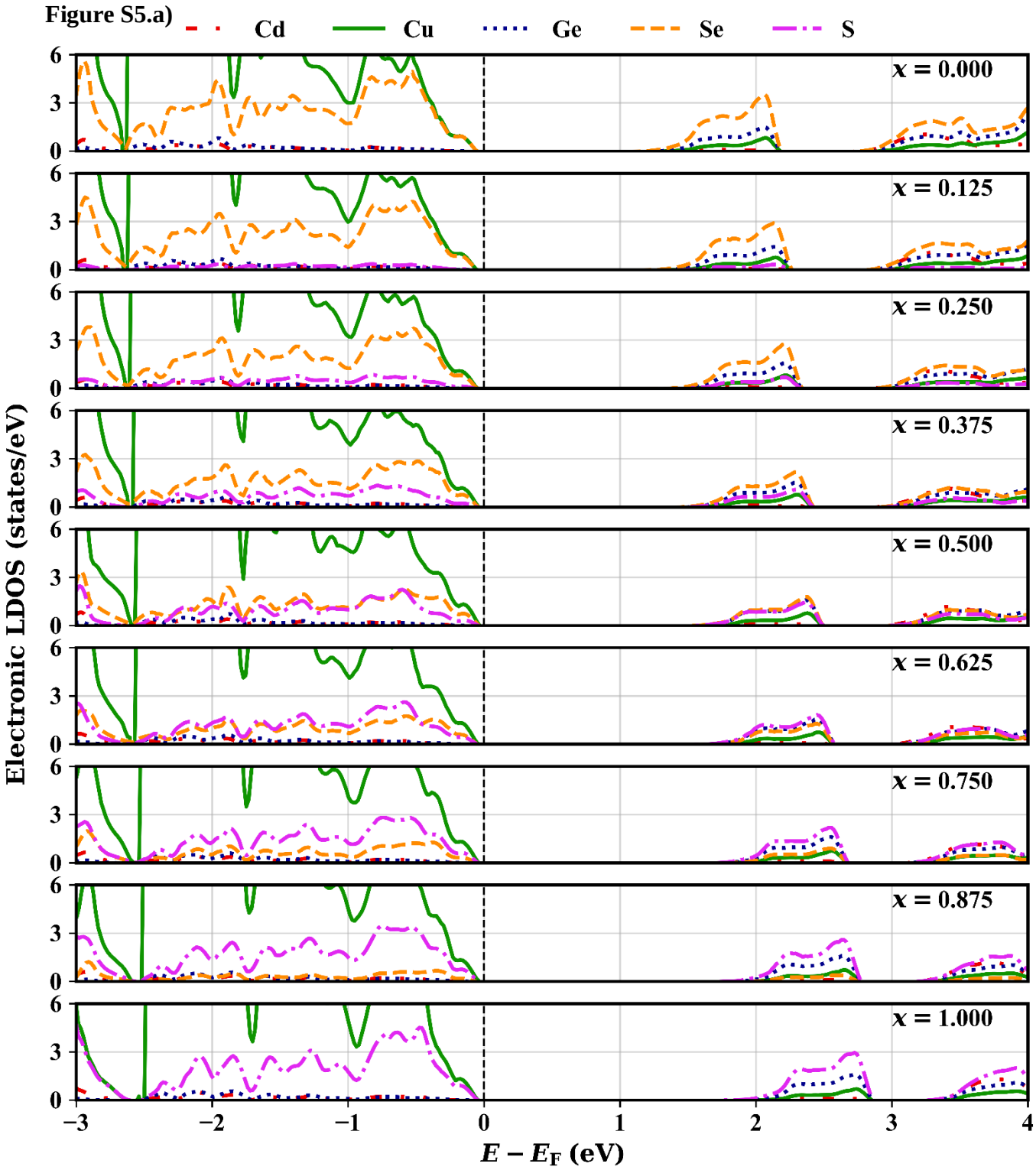

Figure S5 (a-b). LDOS plots for tetragonal (t-) and orthorhombic (o-) $Cu_2CdGe(S_xSe_{1-x})_4$. **(a)** t-$Cu_2CdGe(S_xSe_{1-x})_4$, **(b)** o-$Cu_2CdGe(S_xSe_{1-x})_4$.

Figure S5.b)

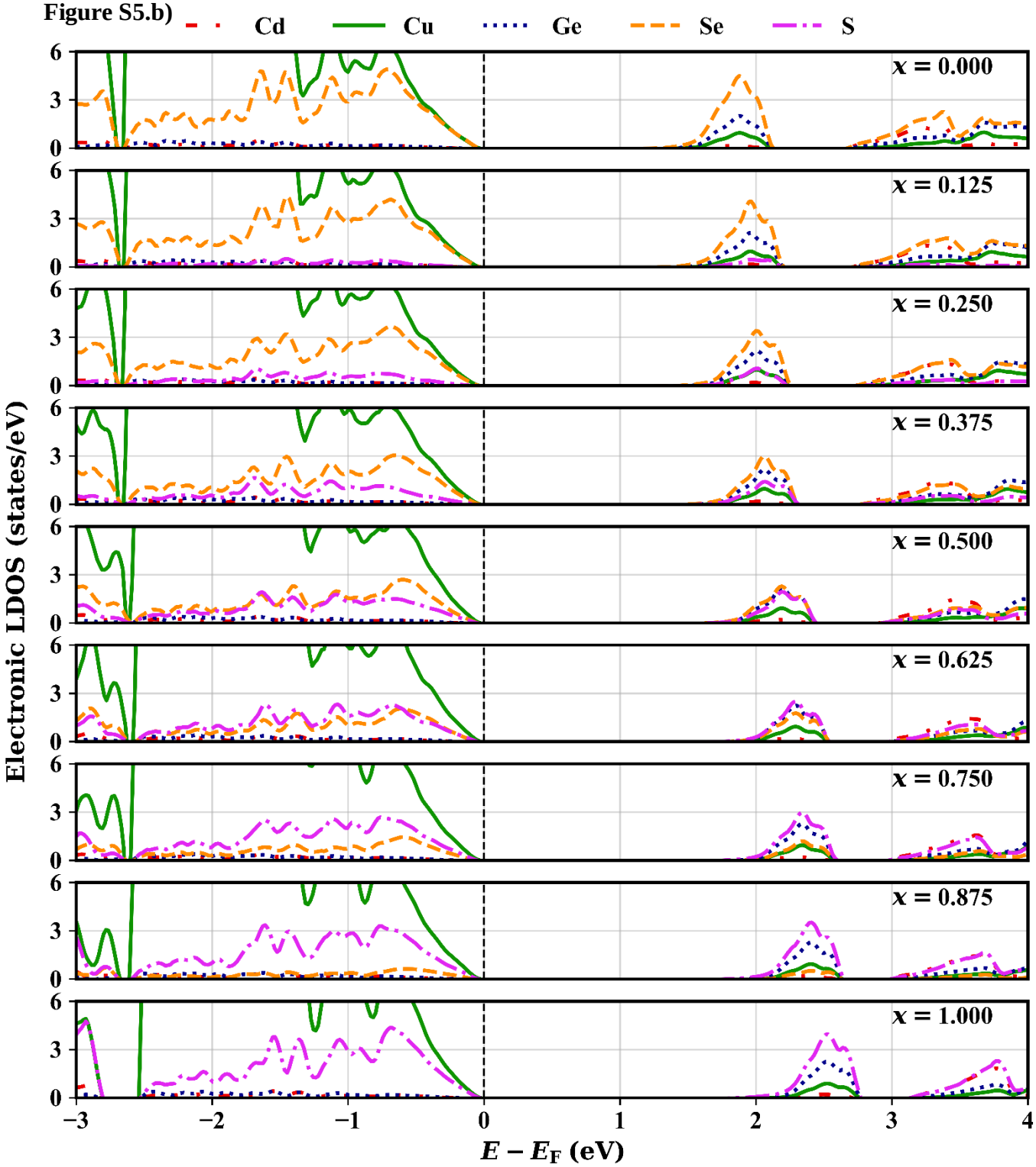
Cd
Cu
Ge
Se
S
x = 0.000
x = 0.125
x = 0.250
x = 0.375
x = 0.500
x = 0.625
x = 0.750
x = 0.875
x = 1.000
Electronic LDOS (states/eV)
E − E_F (eV)

Figure S6.a)

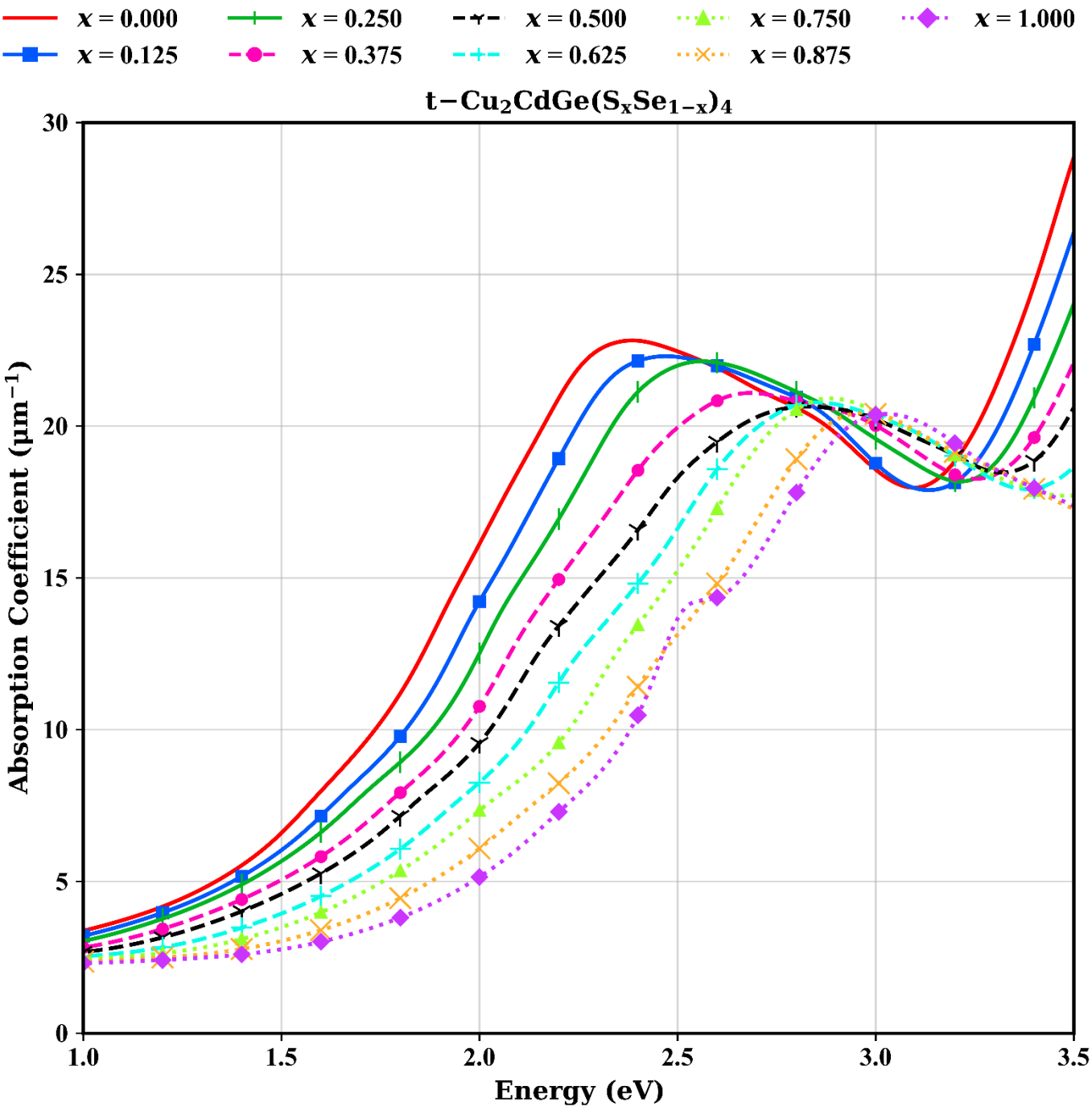

Figure S6 (a-d). Optical properties of tetragonal (t-) and orthorhombic (o-) $Cu_2CdGe(S_xSe_{1-x})_4$ in the energy range of interest for PV applications. Optical response functions are found to be independent of orientation. **(a)** Absorption coefficient for the t-phase, **(b)** Reflectivity for the t-phase, **(c)** Absorption coefficient for the o-phase, **(d)** Reflectivity for the o-phase.

Figure S6.b)

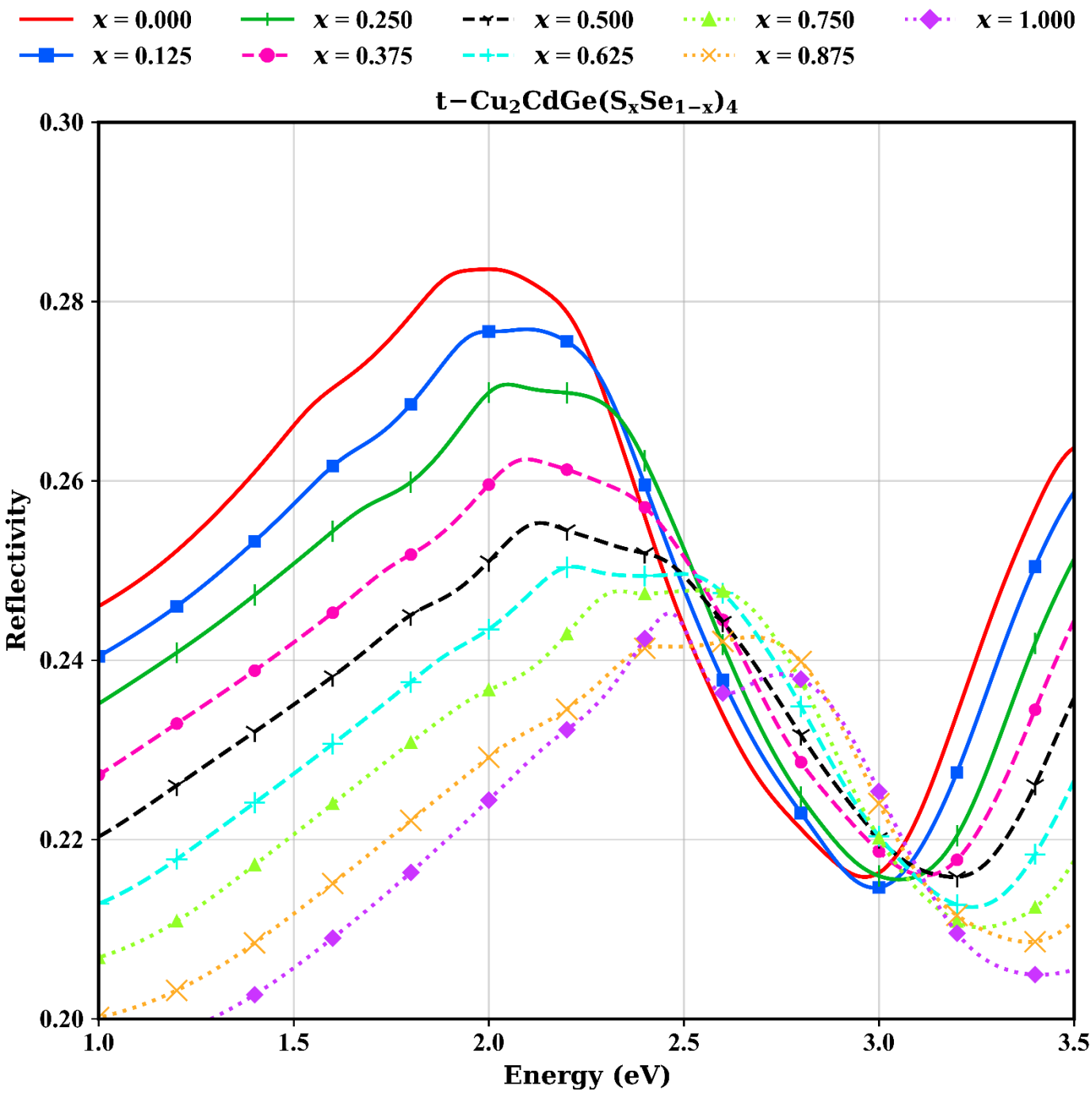
x = 0.000
x = 0.125
x = 0.250
x = 0.375
x = 0.500
x = 0.625
x = 0.750
x = 0.875
x = 1.000
t−Cu2CdGe(SxSe1−x)4
Reflectivity
Energy (eV)
0.30
0.28
0.26
0.24
0.22
0.20
1.0
1.5
2.0
2.5
3.0
3.5

Figure S6.c)

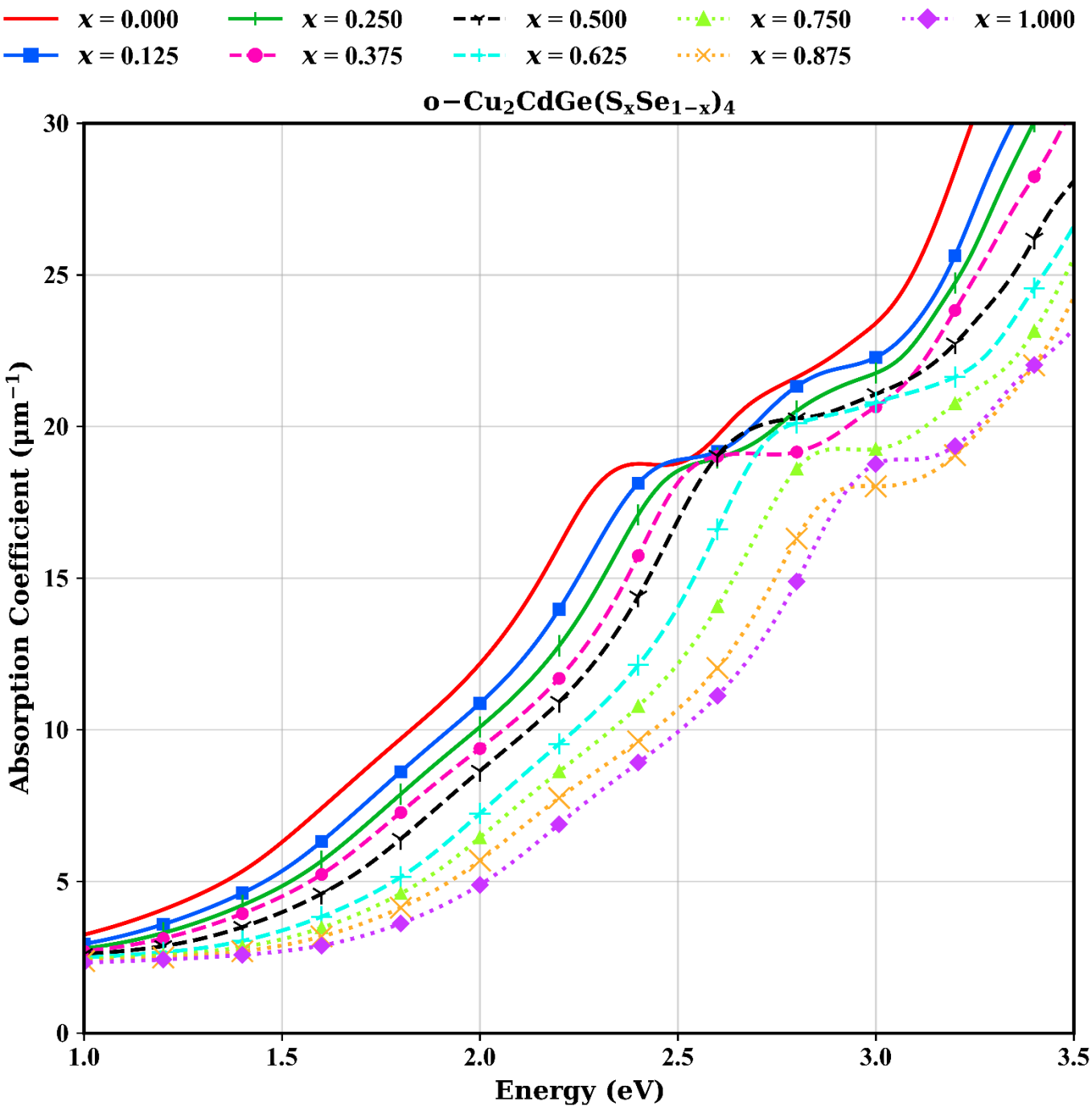
x = 0.000
x = 0.125
x = 0.250
x = 0.375
x = 0.500
x = 0.625
x = 0.750
x = 0.875
x = 1.000
o−Cu2CdGe(SxSe1−x)4
Absorption Coefficient (μm−1)
Energy (eV)
0
5
10
15
20
25
30
1.0
1.5
2.0
2.5
3.0
3.5

Figure S6.d)

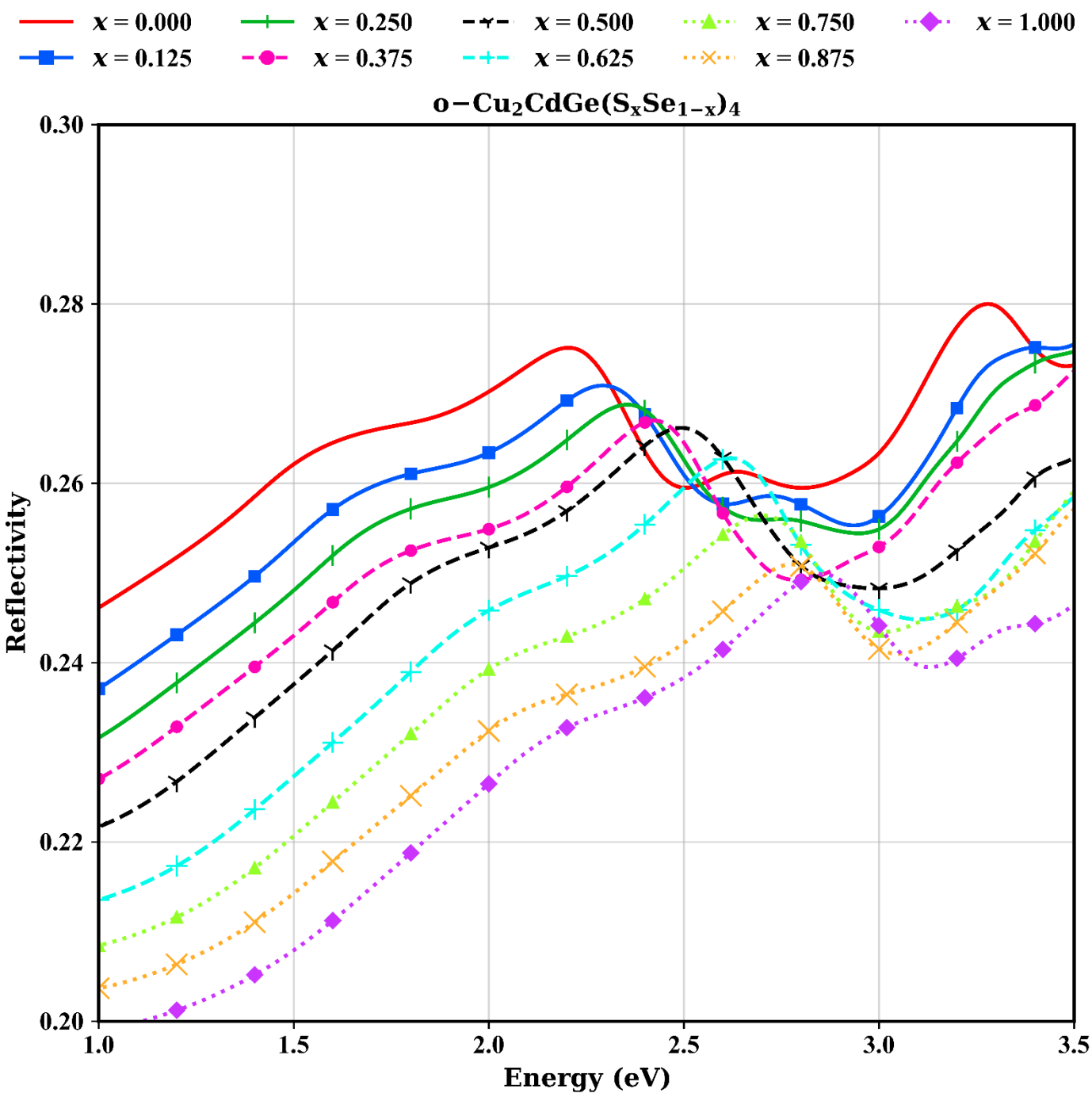
x = 0.000
x = 0.125
x = 0.250
x = 0.375
x = 0.500
x = 0.625
x = 0.750
x = 0.875
x = 1.000
o−Cu2CdGe(SxSe1−x)4
Reflectivity
Energy (eV)
0.30
0.28
0.26
0.24
0.22
0.20
1.0
1.5
2.0
2.5
3.0
3.5

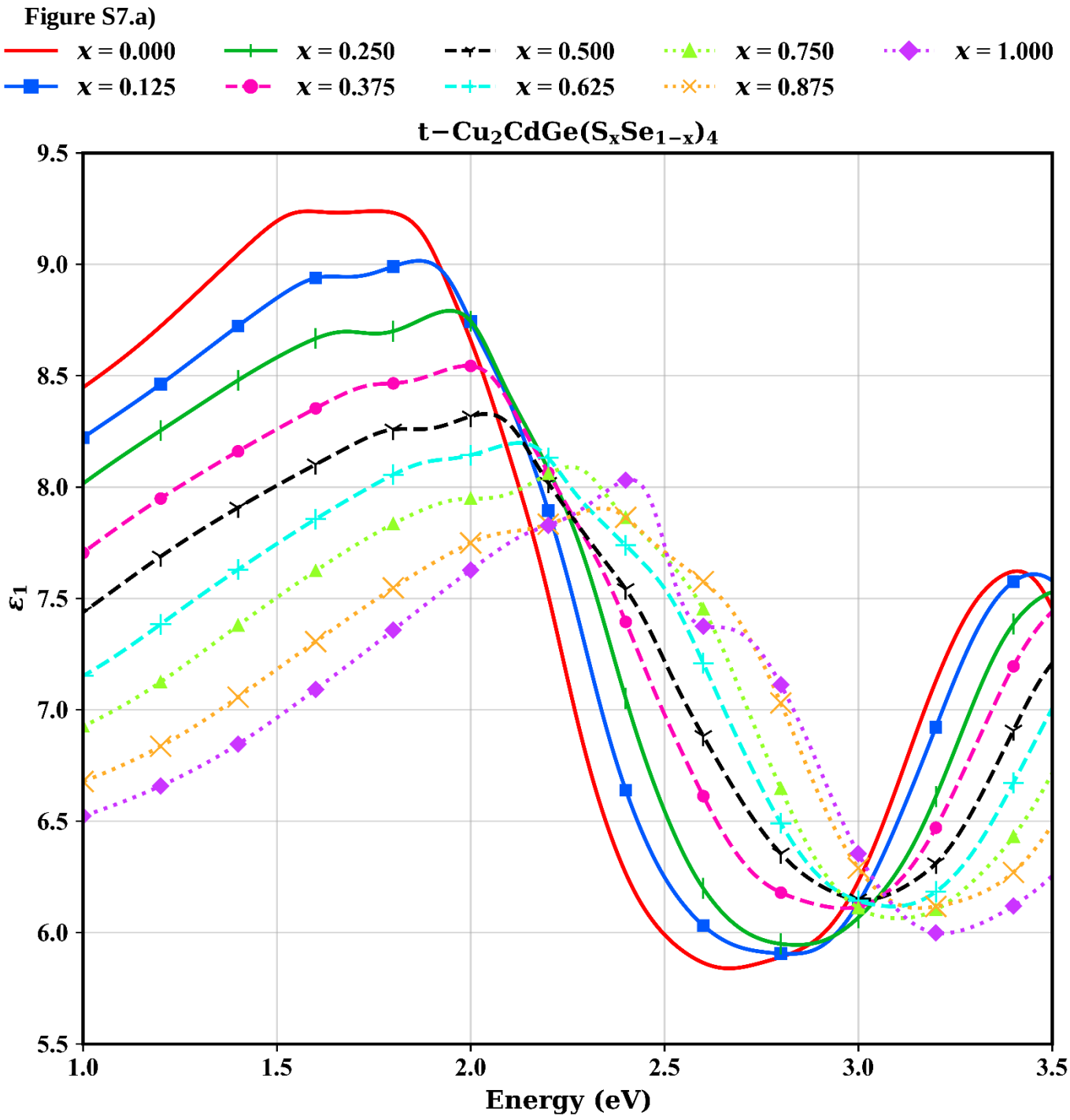

Figure S7 (a-d). Complex dielectric function in tetragonal (t-) and orthorhombic (o-) $Cu_2CdGe(S_xSe_{1-x})_4$. **(a)** Real part ε_1 for the t-phase, **(b)** Imaginary part ε_2 for the t-phase, **(c)** Real part ε_1 for the o-phase, **(d)** Imaginary part ε_2 for the o-phase.

Figure S7.b)

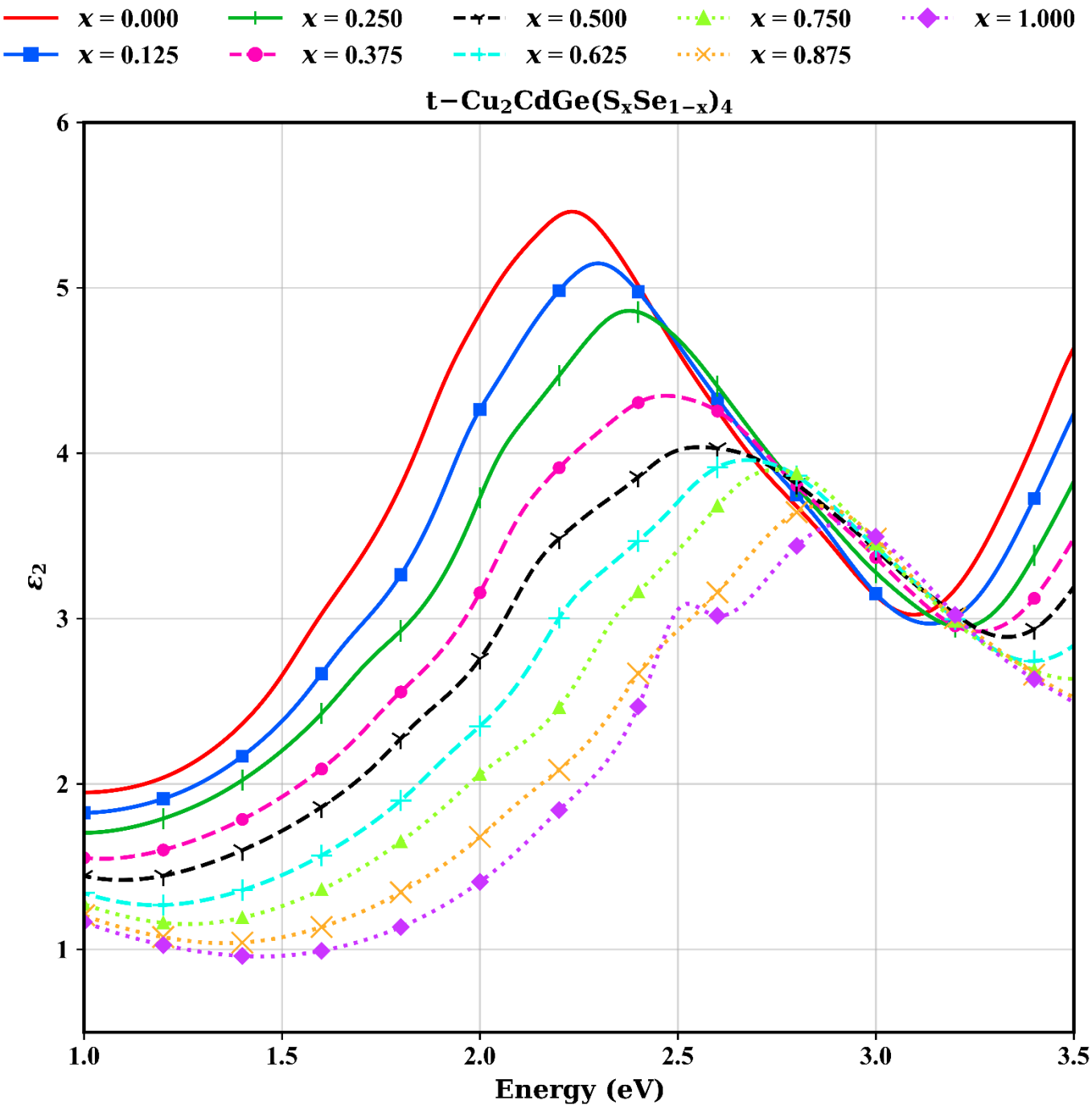
x = 0.000
x = 0.125
x = 0.250
x = 0.375
x = 0.500
x = 0.625
x = 0.750
x = 0.875
x = 1.000
t−Cu2CdGe(SxSe1−x)4
ε2
Energy (eV)
1
2
3
4
5
6
1.0
1.5
2.0
2.5
3.0
3.5

Figure S7.c)

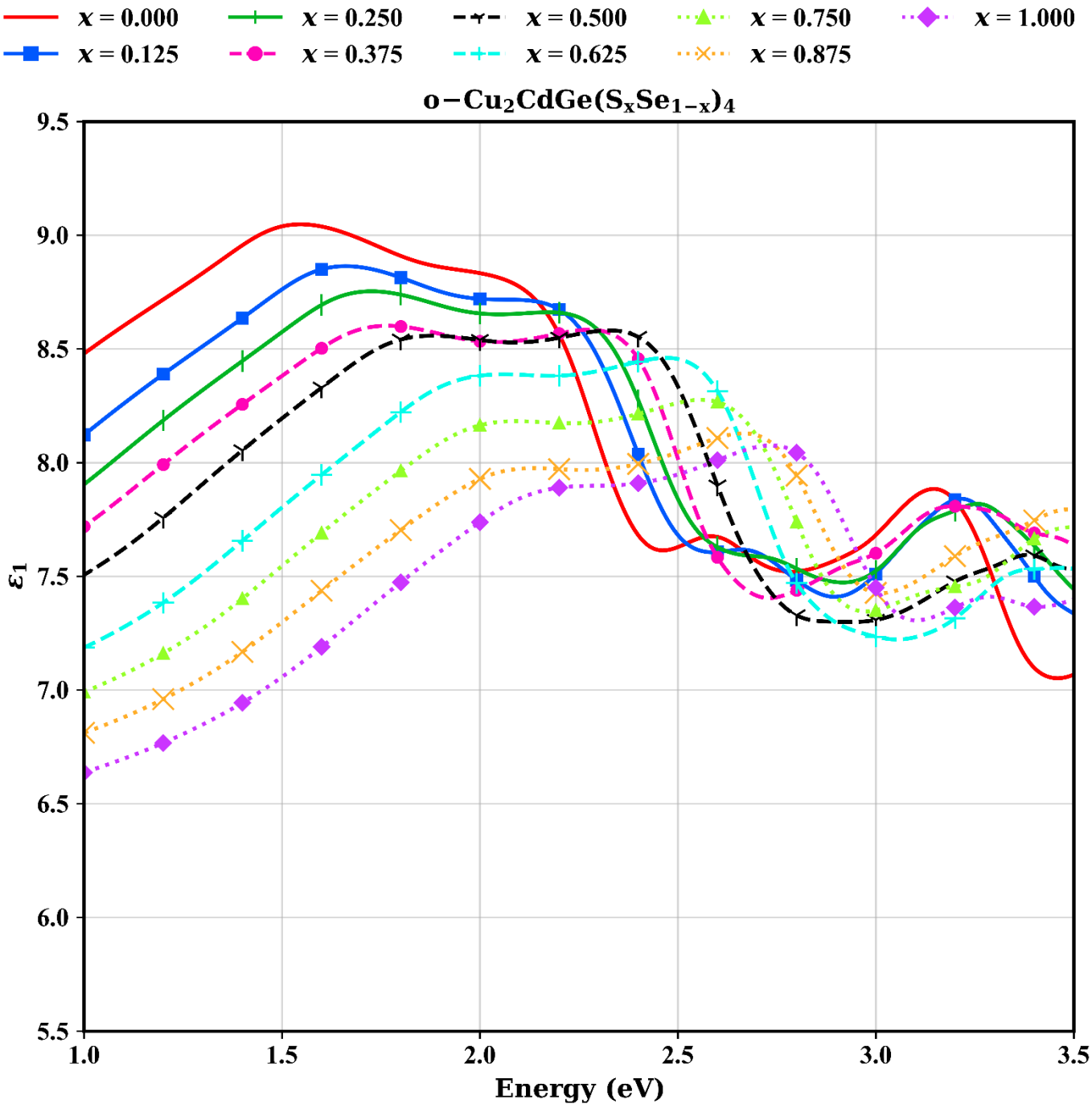
x = 0.000
x = 0.125
x = 0.250
x = 0.375
x = 0.500
x = 0.625
x = 0.750
x = 0.875
x = 1.000
o−Cu2CdGe(SxSe1−x)4
ε1
Energy (eV)
9.5
9.0
8.5
8.0
7.5
7.0
6.5
6.0
5.5
1.0
1.5
2.0
2.5
3.0
3.5

Figure S7.d)

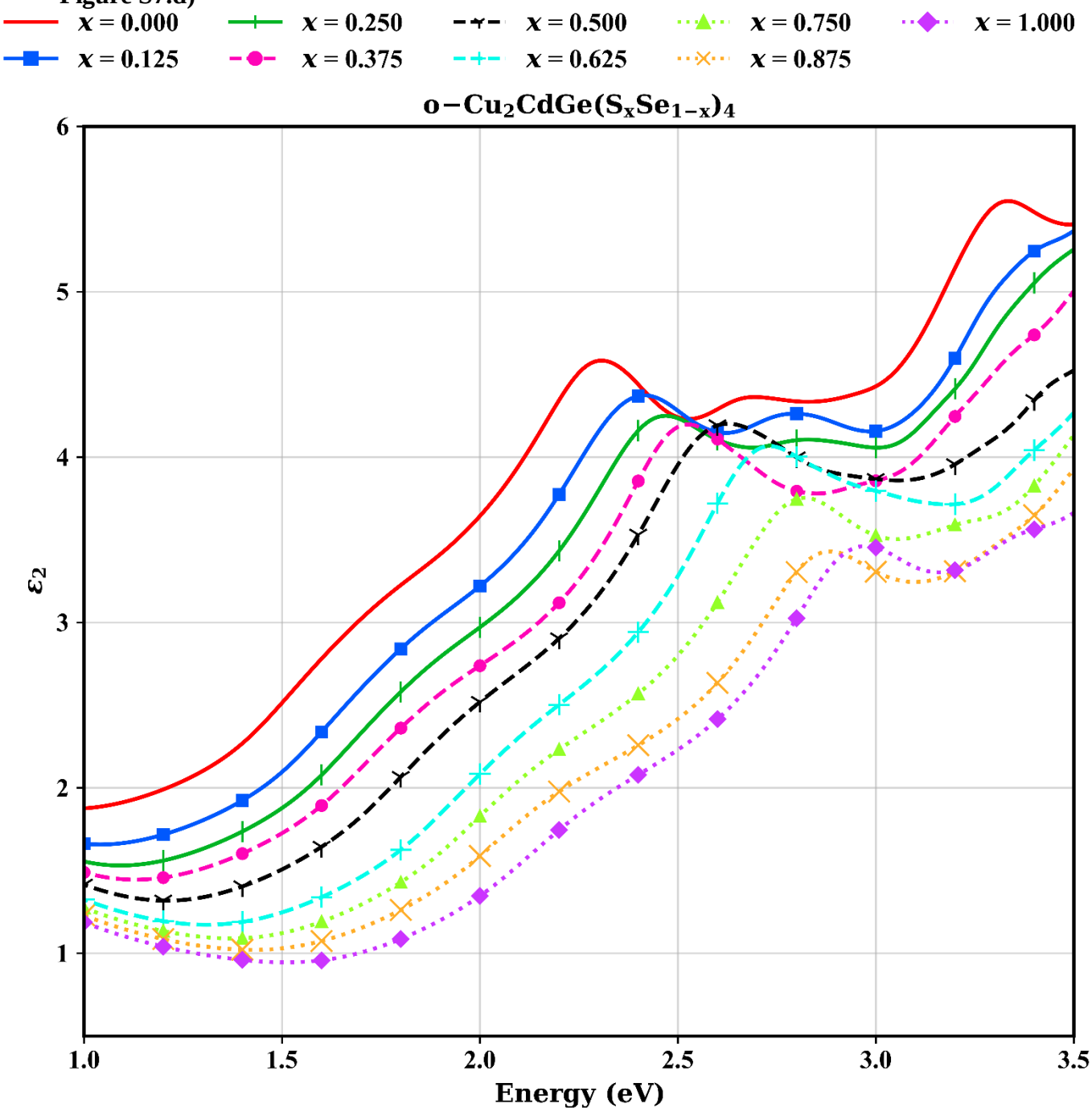
x = 0.000
x = 0.125
x = 0.250
x = 0.375
x = 0.500
x = 0.625
x = 0.750
x = 0.875
x = 1.000
o−Cu2CdGe(SxSe1−x)4
ε2
Energy (eV)
1
2
3
4
5
6
1.0
1.5
2.0
2.5
3.0
3.5

References

[1] X. Li, M. Pilvet, K. Timmo, M. Grossberg, V. Mikli, and M. Kauk-Kuusik, *The Effect of S/Se Ratio on the Properties of $Cu_2CdGe(S_xSe_{1-x})_4$ Microcrystalline Powders for Photovoltaic Applications*, Solar Energy **209**, 646 (2020).

[2] H. Matsushita, T. Ichikawa, and A. Katsui, *Structural, Thermodynamical and Optical Properties of Cu_2-II-IV-VI_4 Quaternary Compounds*, J Mater Sci **40**, 2003 (2005).

[3] J. Krustok, T. Raadik, X. Li, M. Kauk-Kuusik, K. Timmo, S. Oueslati, and M. Grossberg, *Study of Point Defects in Wide-Bandgap Cu_2CdGeS_4 Microcrystals by Temperature and Laser Power Dependent Photoluminescence Spectroscopy*, J. Phys. D: Appl. Phys. **53**, 275102 (2020).

[4] M. Kauk-Kuusik, X. Li, M. Pilvet, K. Timmo, M. Grossberg, T. Raadik, M. Danilson, V. Mikli, M. Altosaar, J. Krustok, and J. Raudoja, *Study of $Cu_2CdGeSe_4$ Monograin Powders Synthesized by Molten Salt Method for Photovoltaic Applications*, Thin Solid Films **666**, 15 (2018).

[5] T. V. Vu, A. A. Lavrentyev, B. V. Gabrelian, K. D. Pham, C. V. Nguyen, K. C. Tran, H. L. Luong, M. Batouche, O. V. Parasyuk, and O. Y. Khyzhun, *Electronic, Optical and Elastic Properties of $Cu_2CdGeSe_4$: A First-Principles Study*, Journal of Elec Materi **48**, 705 (2019).

[6] Y. Zhang, X. Sun, P. Zhang, X. Yuan, F. Huang, and W. Zhang, *Structural Properties and Quasiparticle Band Structures of Cu-Based Quaternary Semiconductors for Photovoltaic Applications*, Journal of Applied Physics **111**, 063709 (2012).